Neoplasia 39 (2023) 100896

Contents lists available at ScienceDirect

Neoplasia

journal homepage: www.elsevier.com/locate/neo

The promise of metabolic imaging in diffuse midline glioma

Samantha Lovibond[a,1], Alexandra N. Gewirtz[b,1], Luca Pasquini[a], Simone Krebs[a,c,d,2], Maya S. Graham[b,2,*]

[a] Molecular Imaging and Therapy Service, Department of Radiology, Memorial Sloan Kettering Cancer Center, New York, NY, USA
[b] Department of Neurology, Memorial Sloan Kettering Cancer Center, New York, NY, USA
[c] Radiochemistry and Imaging Sciences Service, Department of Radiology, Memorial Sloan Kettering Cancer Center, New York, NY, USA
[d] Department of Radiology, Weill Cornell Medical College, New York, NY 10065, USA

ARTICLE INFO

Keywords:
Diffuse midline glioma
Metabolism
PET
MRI
Imaging

ABSTRACT

Recent insights into histopathological and molecular subgroups of glioma have revolutionized the field of neuro-oncology by refining diagnostic categories. An emblematic example in pediatric neuro-oncology is the newly defined *diffuse midline glioma (DMG), H3 K27–altered.* DMG represents a rare tumor with a dismal prognosis. The diagnosis of DMG is largely based on clinical presentation and characteristic features on conventional magnetic resonance imaging (MRI), with biopsy limited by its delicate neuroanatomic location. Standard MRI remains limited in its ability to characterize tumor biology. Advanced MRI and positron emission tomography (PET) imaging offer additional value as they enable non-invasive evaluation of molecular and metabolic features of brain tumors. These techniques have been widely used for tumor detection, metabolic characterization and treatment response monitoring of brain tumors. However, their role in the realm of pediatric DMG is nascent. By summarizing DMG metabolic pathways in conjunction with their imaging surrogates, we aim to elucidate the untapped potential of such imaging techniques in this devastating disease.

Introduction

Brain tumors are the leading cause of pediatric cancer deaths, and diffuse midline gliomas (DMG) are among the most deadly [1]. Advances in our understanding of the underlying genetic abnormalities in these tumors led to the creation of a distinct diagnostic entity, *diffuse midline glioma (DMG) with histone H3K27M mutation*, in the 2016 World Health Organization (WHO) Classification of Tumors of the Central Nervous System [2]. This was updated to *diffuse midline glioma, H3 K27-altered,* in the 2021 WHO Classification to reflect convergent mechanisms of K27 modification such as EZHIP overexpression [3]. This group of tumors, characterized by midline location and K27M mutations in histone H3 genes, includes the majority of tumors previously referred to as diffuse intrinsic pontine glioma (DIPG). As terminology has shifted significantly over the last decade, for the purpose of this review, we will consider studies including tumors classified as DMG, DIPG, and brain stem diffuse astrocytoma or glioma by clinico-radiographic criteria, even when H3K27M status was not determined.

As biopsy or resection is often not possible due to the location of DMG, the diagnosis is typically based on clinical and neuroradiological findings. Standard magnetic resonance imaging (MRI) remains limited in its ability to characterize tumor identity and define functionally active disease, leading to interest in advanced imaging modalities as an adjunct. Metabolic imaging modalities are of particular interest, as they may allow for non-invasive interrogation of DMG biology. Here, we review the clinical characteristics and metabolic alterations of DMG and discuss the current state of metabolic imaging techniques employed to non-invasively diagnose and monitor these aggressive tumors.

DMG clinical characteristics

DMG afflicts 300-400 patients in the United States annually [1]. It predominantly affects young children, peaking at 6-10 years of age [4], though it can rarely affect adults as well. Median overall survival (OS) in DMG is unfortunately less than a year, with <10% of patients surviving two years [5]. In a retrospective study, median OS for adult DMG

Abbreviations: DMG, diffuse midline glioma; DIPG, diffuse intrinsic pontine glioma; MRI, magnetic resonance imaging; PET, positron emission imaging; MRS, magnetic resonance spectroscopy; MRP, magnetic resonance perfusion.

* Corresponding author at: 1275 York Ave, Box 52, New York, NY 10065.
E-mail address: grahamm3@mskcc.org (M.S. Graham).

[1] Contributed equally as first authors
[2] Contributed equally as senior authors

https://doi.org/10.1016/j.neo.2023.100896
Received 14 October 2022; Received in revised form 10 February 2023; Accepted 13 March 2023

patients was 16 months as compared to 5 months for pediatric patients, indicating a worse prognosis for children [6].

DMG by definition involves the midline structures of the central nervous system, including the thalamus, brainstem and spinal cord, with the pons being the most common location [7]. Diffuse infiltration of the brainstem is commonly seen, especially in pontine tumors. Approximately 25% of DMG invade the thalamus and upper cervical cord as well [8]. More rarely, DMG is identified in other midline structures. In a review of 47 DMG cases, six arose in other sites including the hypothalamus, third ventricle, pineal region and cerebellum [9].

Given its midline predilection, symptoms attributable to the brainstem are a hallmark of DMG. The classical clinical triad consists of cerebellar dysfunction such as ataxia, long tract signs such as hemiparesis and cranial neuropathies [10], with cranial nerves VI and VII most commonly affected. Symptoms of increased intracranial pressure are seen in <10% of patients at presentation and are typically due to functional obstruction [11]. Given the aggressive nature of these tumors, symptom duration is usually short, with presentation within 3 months of symptom onset.

Due to the eloquent location of DMG tumors, surgical resection is rarely feasible. Standard treatment for newly diagnosed DMG is local radiotherapy, with a survival benefit of approximately 3 months [12]. Radiation is routinely combined with temozolomide or other experimental agents, though no chemotherapy regimen to date has demonstrated a meaningful benefit [13]. The elucidation of the molecular underpinnings of DMG has generated interest in novel therapeutic strategies blocking the specific molecular pathways and epigenetic alterations driving DMG biology.

Hallmark DMG genetics

The characteristic genetic alteration of DMG is a lysine-to-methionine substitution at position 27 (K27M) in one of the histone H3 variants [14]. It is most frequently seen in histone H3.3, with a minority of cases involving histone H3.1 or more rarely H3.2 [15]. These oncohistone variants define DMG subgroups with distinct anatomic localization, ages of onset and prognoses, with H3.1/3.2K27M tumors restricted to the pons in younger children and with longer median OS [15]. Oncohistone variants also display discrete concurrent mutations. Platelet derived growth factor receptor A (*PDGFRA*) amplifications are commonly associated with H3.3K27M, while activin A receptor type 1 (*ACVR1*) activating mutations are associated with H3.1K27M [16]. *TP53* pathway mutations (including *PPM1D*) are frequently observed in all histone-mutant tumor subgroups. While rarely reported, there have been documented co-occurrences of H3K27M mutations with targetable mutations considered disease defining in other gliomas. Recent retrospective series characterizing the molecular landscape of DMG have found variable rates of concurrent BRAF V600E mutations, detected in 5-10% of tested cases [9,17,18]. This most recent series found a higher rate of concurrent FGFR1 mutation, seen in 9/55 DMG tumors (16.4%) [18]. There have also been reported cases of concurrent IDH1 R132X mutations, with 2 of 43 (4.7%) infratentorial IDH-mutant tumors also harboring H3.3 K27M mutations [19]. These rates of detection may suggest that secondary driver mutations are not looked for frequently enough, though a large sequencing study of 164 DMGs found no cases of concurrent BRAF V600E or IDH1 R132X [20], confirming the relative rarity of secondary driver mutations.

H3K27M mutation causes a global reduction in trimethylation at H3K27 (H3K27me3) [21]. This repressive chromatin mark is catalyzed by the Polycomb repressive complex 2 (PRC2), whose activity is impaired in the setting of H3K27M. However, there is also a gain of H3K27me3 at loci of strong Polycomb targets due to impaired PRC2 spreading [21]. Activating chromatin marks like H3K27 acetylation are impacted by H3K27M as well [22]. These epigenetic alterations drive upregulation of genes involved in neural development, promoting self-renewal capacity and impairing differentiation [14] in the appropriate cellular context. These global changes are true of both H3.3 and H3.1K27M tumors, though more subtle differences in their chromatin reprogramming and consequent gene expression profiles have been delineated [23].

Overall, DMGs are aggressive incurable tumors with distinct clinical trajectories and biologies defined by hallmark mutations in histone H3 variants. As these tumors reside in predominantly surgically inaccessible regions of the brain, noninvasive correlates of their genetics, metabolism and clinical behavior both at diagnosis and during treatment are an urgent unmet clinical need. Advanced metabolic imaging is one such noninvasive approach that stands to make a substantial clinical impact in this patient population. A better understanding of the metabolic hallmarks of this disease will only amplify this potential impact.

DMG metabolic insights

The metabolic implications of epigenetic modification in H3K27-altered DMG are starting to be unraveled. These metabolic insights may uncover therapeutic vulnerabilities that allow for improved targeted treatments for DMG (Figure 1A). Metabolic adaptation has long been recognized as a key component of tumorigenesis. The Warburg effect, or aerobic glycolysis, is the most notable example, where tumor cells preferentially shunt glucose to lactate even in the presence of ample oxygen [24]. DMG-derived cell lines show increased glycolysis and decreased oxidative phosphorylation [25]. A sizeable cohort of pediatric high-grade gliomas, including DMGs, demonstrated decreased mitochondrial DNA (mtDNA) content as compared with normal brain, suggesting a possible molecular basis for aerobic glycolysis. Restoring mtDNA levels and shifting DMG cells towards oxidative phosphorylation via pharmacologic stimulation had cytotoxic effects [25]. Comprehensive profiling of isogenic K27M mutant versus wild-type (WT) neural stem cells as well as patient-derived cell lines revealed glycolysis and related metabolic pathways such as the tricarboxylic acid (TCA) cycle and glutaminolysis as the top upregulated pathways [26]. These results were confirmed in pediatric glioma transcriptomic databases. Elevated glucose or glutamine metabolism supported elevated α-ketoglutarate (α-KG) levels, which potentiated global H3K27 demethylation, linking altered metabolism and epigenetics. Targeting enzymes that produce α-KG prolonged survival in preclinical xenograft models. Importantly, noninvasive imaging with magnetic resonance spectroscopy (MRS) in fifteen patients with midline gliomas confirmed significantly higher citrate (a TCA cycle component) and glutamine levels in K27-mutant gliomas [26], suggesting that metabolic rewiring in DMG can be leveraged for imaging purposes.

The unique biology of DMGs also results in unique metabolic susceptibilities. Transcriptomic profiling of a syngeneic H3K27M DMG mouse model identified methionine metabolism as a main upregulated pathway in the H3K27M context [27]. Genetic and pharmacologic screening of isogenic cells revealed an imbalance in methionine metabolic pathways as the key driver of this dependency, with reduced levels of a core methionine cycle enzyme (MAT2A) and increased levels of a core methionine salvage pathway enzyme (AMD1). MAT2A converts methionine to S-adenosyl methionine (SAM), an important co-substrate for methyl group transfers such as histone methylation, again linking metabolism and epigenetics. This methionine metabolism imbalance could be exploited therapeutically, with both methionine diet restriction and MAT2A inhibition impeding DMG growth in their preclinical model [27]. Altered methionine metabolism might also serve as a basis for DMG metabolic imaging with ^{11}C-methyl-L-methionine (^{11}C-MET) PET (Figure 1B), though this specific relationship has not yet been explored clinically. AMD1 upregulation has additional metabolic implications, as this enzyme is also critical to polyamine synthesis. Polyamine synthesis regulators are increased in DMG tumors, though this was independent of K27 mutation status [28]. Simultaneously targeting polyamine biosynthesis and transport prolonged survival in DMG xenograft models [28].

Pyrimidine biosynthesis has also recently emerged as dysregulated in DMG, comprising the top hits in a genome-wide CRISPR screen in sev-

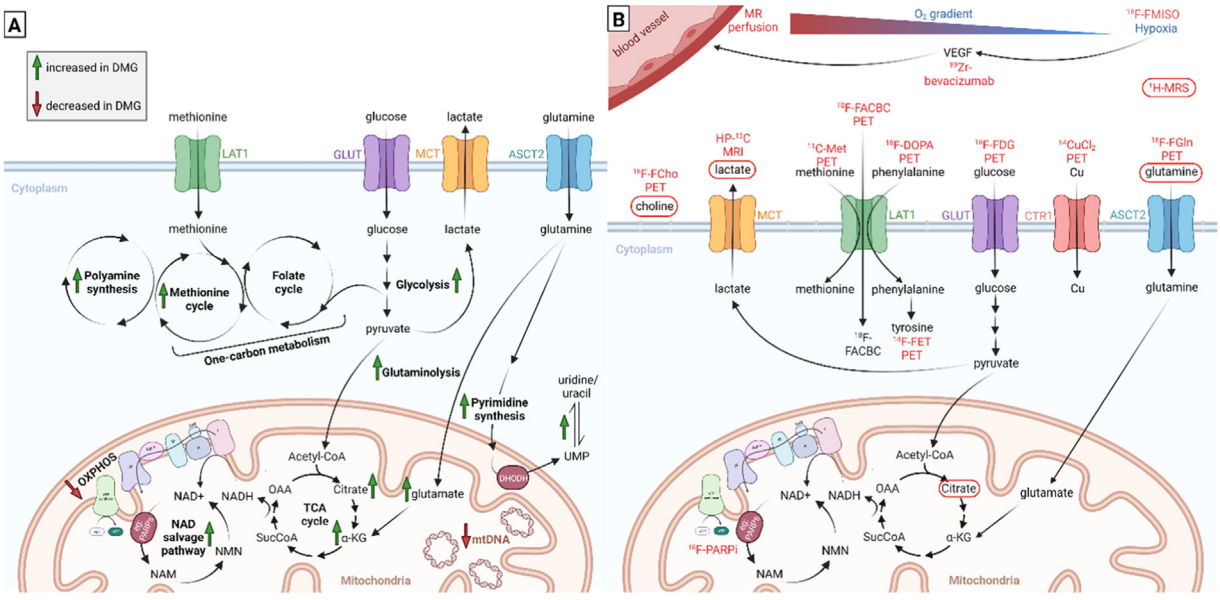

Fig. 1. Cellular metabolism in DMG and in advanced imaging techniques. (A) Summary of altered metabolic pathways in DMG tumors. (B) Schematic of cellular basis of advanced metabolic imaging modalities. *Created with Biorender.com.*

eral DMG cell lines [29]. Inhibition of *de novo* pyrimidine synthesis with a dihydroorotate dehydrogenase (DHODH) inhibitor was cytotoxic only to DMG cells and not adult glioblastoma cells. This dependency is due to a concomitant increase in pyrimidine degradation that limits the ability of DMG cells to utilize the alternate pyrimidine salvage pathway [29]. As glutamine is a precursor to pyrimidine synthesis, DMG pyrimidine dependency suggests that ^{18}F-Fluoroglutamine (^{18}F-FGln) PET might be particularly useful for imaging DMGs (Figure 1B), though no clinical data exists in this patient population. There are also metabolic sensitivities particular to different DMG subtypes. For instance, mutant PPM1D drives silencing of a key regulator of NAD biosynthesis [30]. This promotes reliance on the alternate NAD salvage pathway in PPM1D-mutant DMG, which can be targeted therapeutically to impair DMG growth [30]. This upregulation of the NAD salvage pathway in DMGs can also be utilized for noninvasive imaging, as it correlates with increased expression of NAD+ consumers such as poly (ADP-ribose) polymerases (PARPs) which can be used as PET imaging targets. In a genetically engineered mouse model of DMG, ^{18}F-PARPi PET enabled clear delineation of tumor tissue, with superior signal-to-noise ratio when compared with conventional MRI and other investigational PET tracers [31], suggesting it may have promise for imaging DMG patients as well.

Finally, oncogenic metabolic rewiring is not limited to tumor cell-intrinsic mechanisms. Remodeling of metabolism in the tumor microenvironment is also capable of promoting tumorigenesis. Recent work utilizing both single cell transcriptomic data as well as multiplex immunofluorescence in a cohort of pediatric brain tumors from the Children's Brain Tumor Network (CBTN) dataset demonstrated upregulation of extracellular purine metabolism driven by interaction between tumor cell CD73 and microglial cell CD39 under hypoxic conditions, which has pro-tumorigenic and immunosuppressive consequences [32]. Collectively, these insights into metabolic reprogramming in DMG suggest not only novel therapeutic strategies but also metabolic imaging approaches that can capitalize on the unique biology of these tumors.

Classic imaging characteristics

On conventional MRI, DMG is classically defined as an infiltrative and expansile mass involving midline structures that demonstrates T1-hypointensity and T2-hyperintensity with minimal contrast enhancement [33,34]. Frank hemorrhage and edema are uncommonly seen. The incidence of leptomeningeal dissemination varies widely, reported in 17-56% of patients [35–37], in part due to inconsistent neuraxis surveillance.

However, more recent studies have highlighted the pronounced variability in DMG appearance on MRI, particularly with respect to enhancement or necrosis [34,38]. A retrospective review of 33 pediatric midline glioma patients (both H3K27-altered and WT) found that 67% of pontine gliomas and 50% of thalamic gliomas exhibited contrast enhancement [38]. Similarly, a large study from the International DIPG Registry found that 69% of the 347 DIPGs imaged with contrast showed some enhancement, primarily in a patchy pattern [34]. Contrast enhancement by itself did not significantly predict overall survival, and thus the prognostic value of contrast enhancement in pediatric DMG remains controversial [39]. Necrosis also seems variable in these tumors, though most studies assessing necrosis are radiographic in nature, without histologic corroboration. In one study of 15 adolescent and young adult DMG patients, necrosis with surrounding rim enhancement was seen in 67% of tumors [40]. This was corroborated by a separate study including 24 pediatric K27M-mutant midline gliomas, which found 63% to have central necrosis [38]. In contrast, radiographic necrosis on MRI was found in only 20% of cases in another study of 48 brainstem gliomas, and strongly correlated with shorter survival [41], though this study did not distinguish between H3K27-altered and WT, as only 2 patients had pathology available.

Occasionally, DMG exhibits mild diffusion restriction on diffusion weighted imaging, related to increased cellularity [42,43]. Compared to other aggressive brain neoplasms, diffusion restriction is not a predominant feature of DMG, seen in 60% of cases in one of the largest cohorts published to date [34]. Nevertheless, when present, diffusion restriction may be associated with worse prognosis, possibly demarcating areas of anaplasia within the tumoral tissue [44]. Lower apparent diffusion coefficient (ADC) values, a measure of diffusion restriction, has been reported as an independent predictor of H3K27M mutation in DMG [45], though conflicting results were seen in a separate study, which found higher ADC values in K27-altered DMG [46]. Among H3K27M mutated tumors, diffusion imaging can help further characterize the type of mutation, with generally higher ADC values in the H3.1K27M subtype [47].

The application of artificial intelligence techniques to MRI has shown some potential for providing prognostic imaging markers in brain tu-

mors [48]. In DMG, radiomic analysis of MR images has been used to successfully predict H3K27M mutation [49]. Another recent study correlated more homogeneous DMG texture on T2W images with worse prognosis [50]. Although texture analysis may be helpful in the initial detection of DMG, there are still no validated MRI biomarkers for therapeutic response/resistance, progression, or overall survival (OS) [34].

Advanced MRI techniques

Advanced MRI techniques may offer some improvement on conventional MRI in the diagnosis and surveillance of DMG. These include MR perfusion approaches, MR Spectroscopy and hyperpolarized MR.

Magnetic resonance perfusion (MRP)

MRP is an advanced MRI technique aimed at imaging vascularity in the brain [51]. Several MRP approaches have been established to date, including dynamic susceptibility contrast (DSC)-MRI, dynamic contrast enhanced (DCE)-MRI, and arterial-spin labelling (ASL) techniques [52]. DSC-MRI is the most employed technique for clinical evaluation of perfusion in brain tumors [53] and has demonstrated high correlation with tumor grade in gliomas [54,55]. Both DCE-MRI and DSC-MRI techniques involve the intravenous injection of gadolinium-based contrast agents, which are paramagnetic contrasts. DSC-MRI relies on $T2^*$ sequences, which are susceptible to the paramagnetic effect of the contrast bolus, resulting in signal loss caused by its passage in the blood vessels [56]. The processing of the signal intensity curve resulting from the passage of contrast over time provides relative hemodynamic measures, such as cerebral blood volume (CBV), cerebral blood flow (CBF), mean transit time (MTT), time to peak (TTP) [57]. Conversely, DCE-MRI relies on the observation of contrast-induced T1 shortening in the blood-pool and extravascular space, where the contrast may accumulate depending on the permeability of the blood-brain barrier (BBB) [56]. DCE-MRI can provide absolute measures of plasma volume (Vp: measure of the vascular bed), extra plasmatic volume (Ve: measure of the interstitial space), and blood vessel permeability (Ktrans) [56]. ASL enables the measurement of brain perfusion noninvasively at the tissue level without the administration of exogenous contrast [58]. ASL relies on the labeling of inflowing blood protons through magnetic pulses prior to their entry into the tissue of interest. The blood is labeled in the neck and imaged within the brain vasculature through rapid MRI sequences, such as echo-planar imaging. CBF is the most commonly derived parameter from ASL used to assess perfusion [58].

MRP parameters serve as surrogate markers of tumor vasculature, with relevant applications in the diagnosis and prognosis of brain tumors, such as glioma grading, differentiation of tumor recurrence, pseudo-progression, pseudo-response, and radiation necrosis [56]. Several studies support the prognostic value of MRP in DMG. Higher CBV values from DSC-MRI may correlate with H3K27M mutation [45], providing guidance for biopsy procedures. Calmon et al. assessed a group of 27 pediatric DMG patients with either H3.1K27M or H3.3K27M mutated tumors and demonstrated that H3.1K27M mutants have lower perfusion values than H3.3K27M mutants [47]. Pseudoprogression of pontine gliomas may display greater increase of ASL-CBF following standard treatment compared with true progression, improving the accuracy of their differential diagnosis [59]. MRP can depict spatial heterogeneity in tumor vascularity [60] and antiangiogenic treatment effects [60]. MRP has been used to study the tumor microenvironment, by identifying compartments of tissue characterized by different vascularization (tumor habitats), which correlated with patient's survival [61]. Perfusion imaging may also be considered an indirect measure of metabolism, particularly given the relationship between tumor vascularity, tissue oxygenation and metabolic activity [62]. Relative cerebral blood flow (rCBV) has been shown to be correlated with ^{18}F-fluorodeoxyglucose (^{18}F-FDG) [63] and ^{11}C-MET [64,65] avidity in prior studies of glioma patients.

Magnetic resonance spectroscopy (MRS)

Magnetic Resonance Spectroscopy (MRS) is an advanced MRI technique used to investigate tissue metabolites and tumor biology [66]. MRS can assess brain abnormalities microscopically by quantifying cellular metabolites and studying their tissue distribution. The most widely used MRS technique is proton (^{1}H; hydrogen) spectroscopy, which can identify the presence of several metabolites in the brain, shown as peaks in the MRI spectra [67]. The position of the peaks along the x (horizontal) axis displays the chemical shift of the metabolites measured in part per million (ppm), while peak height and area under the curve are related to metabolite concentration.

Standard metabolites measured in the human brain include Choline (Cho, 3.2ppm, cell membrane marker), creatinine (Cr, 3ppm, energy metabolism marker), N-acetyl aspartate (NAA, 2ppm, neuronal marker), lactate (Lac, 1.3ppm, product of anaerobic glycolysis), and lipids (Lip, 0.9-1.4ppm, neuronal destruction/necrosis). Theoretically, malignant lesions demonstrate high Cho:Cr and Cho:NAA ratios due to the rapid turnover of cell membranes increasing Cho and the destruction of normal neurons decreasing NAA [66]. Increased Lip signal on ^{1}H-MRS may indicate necrosis as it is a constituent of cell walls and is increased as a product of cell membrane destruction [33,66]. Lac is increased in the setting of increased glycolysis, seen in many tumors. Before considering ^{1}H-MRS as a diagnostic tool for pediatric DMG, it is noted that this modality has limited spatial resolution of $1cm^3$ or less, and is more technically challenging in the posterior fossa, which may limit its utility for early detection of smaller lesions. Nonetheless, ^{1}H-MRS may have some applications in DMG. A pilot ^{1}H-MRS study in two DIPG patients showed elevated Cho:NAA and Cho:Cr ratios at baseline, with further increased after radiation [68]. A larger prospective study of 36 DIPG patients after radiation therapy found that Cho:NAA from single voxel MRS was predictive of patient outcome in univariate analysis, with increasing Cho:NAA inversely correlated with survival throughout the disease course [69]. ^{1}H-MRS has also be used to detect less common metabolites, such as citrate, in DIPG [70]. At present, no metabolic measures on ^{1}H-MRS at diagnosis have been found to be robust biomarkers of survival in DMG.

Hyperpolarized magnetic resonance imaging/spectroscopy

MRS can detect molecules that exist in certain concentrations (0.5-20 mM); however, many molecules of interest that occur at lower concentrations are left undetected. Hyperpolarization increases the concentration of the ^{13}C labels in the molecules thereby increasing sensitivity and allowing the user to detect molecules of interest occurring at lower concentrations [71] The emergence of ^{13}C-labelled probes, like ^{13}C pyruvate, has enabled real-time in vivo investigations of brain metabolism with [72,73], including adult high-grade gliomas [74]. A pilot study of HP ^{13}C pyruvate MRI/MRS in DMG patients showed this agent is well-tolerated but was unable to comment on clinical utility due to small sample size [75].

Positron emission tomography (PET)

PET co-registered with CT or MRI enables repetitive detection of radiotracer molecules at picomolar concentrations and high spatial anatomical resolution. PET imaging offers additional value to cross-sectional imaging studies in neuro-oncology, as it enables the non-invasive evaluation of molecular and metabolic features of brain tumors [76]. ^{18}F-fluorodeoxyglucose (^{18}F-FDG) is currently the only FDA-approved radiotracer for imaging of brain tumors, though several radiolabeled amino acid tracers have been recently introduced. Procedure and interpretation guidelines for pediatric brain tumor imaging based on the consensus opinion of experienced leaders in the field ensure comparability and repeatability of study results [77].

PET systems provide static, dynamic, or gated images of the distribution of positron-emitting radionuclides within the body by detecting pairs of photons produced by the coincident annihilation of a positron and an electron. Images are produced by a reconstruction process using coincidence pair data. Generally, hybrid imaging is performed with PET/CT or PET/MRI systems, the latter of which is less frequently available, enabling correlative anatomic information and additional tissue characterization. Most clinical brain ^{18}F-FDG PET studies are based on acquisition and visual evaluation of static images. After image acquisition, reconstruction, and calibration, quantitative images are obtained as each pixel represents an activity concentration (Bq/mL). PET parameters for lesion analysis include standardized uptake values (SUVs) such as mean SUV (SUVmean), maximum SUV (SUVmax) (volume encompassing the voxel with highest uptake), and peak SUV (SUVpeak) (approximately 1.2-cm diameter fixed size volume centered on the area with maximum uptake) as measures for the intensity of uptake, and volume-based parameters such as metabolic tumor volume (MTV) (volume encompassed by a defined isocontour around the voxel with the highest PET uptake) and total lesion glycolysis (TLG) (calculated by multiplying MTV by SUVmean) [78]. Furthermore, lesion-to-reference-region ratios using mean or maximum SUV can be used to provide a measure of radiotracer uptake in lesions. For studies using radiolabeled amino-acids static and dynamic acquisition and image analyses are being employed. Dynamic imaging data are analyzed using a tracer kinetic model.

In hybrid PET/CT systems, the radiation exposure depends on the injected activity and on the CT component. The CT component should be optimized for adequate attenuation correction and to avoid unnecessary irradiation. The administered activity should be the lowest possible that guarantees a diagnostic image quality according to the 2016 Update of the North American consensus guidelines for pediatric administered radiopharmaceutical activities [79] and the 2016 EANM Dosage Card [80].

In the following sections, we will summarize data on commonly used clinical PET tracers and introduce novel investigational tracers elucidating different pathways that may afford better characterization of DMG (Table 1).

^{18}F-FDG PET

^{18}F-FDG was the first radiotracer employed for brain tumors PET imaging. ^{18}F-FDG, a positron-emitting analog of glucose, is transported into the cell via glucose transporters, and once inside the cell, it gets phosphorylated by hexokinases, resulting in intracellular retention. Tumor cells frequently overexpress glucose transporters [79], with the GLUT3 isoform predominant in high grade gliomas [81]. The physiologic intense ^{18}F-FDG uptake in brain cortex and basal ganglia, however, limits the sensitivity for detection of brain lesions. Furthermore, ^{18}F-FDG uptake occurs in inflammatory and infectious lesions as well, limiting its specificity.

Few studies have evaluated the role of ^{18}F-FDG PET in patients with DMG, largely focusing on diagnosis and outcome prediction. In a Pediatric Brain Tumor Consortium (PBTC) study of 40 patients with newly diagnosed (ND) diffuse intrinsic brain stem glioma (BSG) receiving baseline ^{18}F-FDG PET prior to a combined radiation therapy regimen, seven patients showed tumor uptake similar to or greater than gray matter (Figure 2) [82]. No association between ^{18}F-FDG uptake intensity and outcome was noted. However, worse survival was noted in children with uptake in at least 50% of the tumor. In another prospective study of 20 patients with ND DIPG, for which 11 patients had baseline ^{18}F-FDG PET in addition to MRI, no correlation of PET parameters with outcome was found, though hyperperfusion on MRI indicated shorter survival [83]. In a larger follow up study by the PBTC with a total of 71 BSG patients, including 53 ND and 18 recurrent (RR) tumors, tumor uptake equal to or above gray matter was seen in 10 patients [84]. While in ND BSG, correlation of tumor contrast enhancement and ^{18}F-FDG uptake suggested worse OS, it suggested more favorable progression-free survival (PFS) in RR BSG. In a more recent PBTC study, baseline ^{18}F-FDG PET and MRI scans of 33 pediatric DIPG patients were pooled from 4 clinical trials evaluating the efficacy of radiation combined with a molecularly targeted therapy [85]. No association between PET parameters and survival was observed. Higher ADC skewness in the contrast-enhanced volume was associated with shorter PFS. Furthermore, a negative correlation between PET and ADC values was noted, with a higher level of negative correlation suggesting a shorter time to progression, which may indicate higher-grade elements within the tumor.

The utility of ^{18}F-FDG PET in guiding stereotactic biopsies has also been investigated. This is of particular importance in pediatric patients with diffuse infiltrative brainstem tumors. Indeed, PET guidance using the region with the highest uptake may improve the diagnostic yield of these biopsies [86].

In summary, DMG are commonly not significantly ^{18}F-FDG avid, and conflicting results regarding the prognostic implications of ^{18}F-FDG avidity have been reported. Explanations for the limited ^{18}F-FDG uptake may rely in the intrinsic tumor heterogeneity, as ^{18}F-FDG uptake is related to anaplastic features [87].

Radiolabeled amino acid PET

In recent years, radiolabeled amino acids such as ^{11}C-methyl-L-methionine (^{11}C-MET), ^{18}F-fluoroethyl-L-tyrosine (^{18}F-FET), and ^{18}F-fluoro-L-dihydroxyphenylalanine (^{18}F-DOPA) have been introduced for brain tumor imaging. Compared to ^{18}F-FDG, these agents offer the distinct advantage of minimal uptake in normal brain, though ^{18}F-DOPA does show physiologic uptake in the basal ganglia. These tracers enter cells through the L-amino acid transporter 1 (LAT1) that is involved in cellular uptake of essential amino acids and overexpressed in gliomas and other tumors [88,89].

^{11}C-MET is the oldest amino acid tracer used for brain tumor imaging, though few studies apply it to DMG. In a retrospective study in 25 patients with diffuse intrinsic BSGs, baseline ^{11}C-MET PET detected a few more lesions than ^{18}F-FDG PET, with a trend toward improved survival in the absence of ^{18}F-FDG and ^{11}C-MET avidity [90]. A recent prospective study with 22 ND DIPG patients showed that baseline ^{11}C-MET PET successfully visualized most tumors (18 of 22; 82%) (Figure 3) [91]. No correlation of imaging metrics and clinical variables with survival outcomes was observed. However, of the patients with initially positive ^{11}C-MET PET scans who experienced local progression (64%), 100% developed recurrent tumors within the initial PET-avid volume. Thus, baseline ^{11}C-MET uptake may delineate regions at increased risk for recurrence.

The diagnostic accuracy and clinical impact of ^{18}F-FET has been recently evaluated in a prospective study in 97 children and adolescents comprising a variety of high- and low-grade tumors, including 6 children with midline glioma with H3K27M mutation [92]. PET scans were performed at primary diagnosis, before or after treatment, or at relapse. Overall, ^{18}F-FET PET showed significantly higher accuracy for detecting tumor in untreated and treated lesions compared to MRI and altered the treatment plan in 33% of patients with clinical indication for additional imaging.

^{18}F-DOPA has gained importance in pediatric oncology, particularly for imaging in children with infiltrative gliomas. ^{18}F-DOPA uptake may enable determination of the *H3K27M* mutation status noninvasively (Figure 4) [93]. Moreover, ^{18}F-DOPA PET might also provide relevant prognostic information in DMG [94]. To date, most studies employed standard static PET parameters such as tumor-to-striatum (T/S) and tumor-to-normal tissue (T/N) ratios. In these studies, the T/S ratio was able to differentiate between mutant and wild-type DMG, superior to advanced MRI-derived diffusion weighted imaging (DWI) and ^{1}H-MRS parameters [46], and was an independent outcome predictor [94]. A recent retrospective study in 15 pediatric brain tumor patients, of which 5 had confirmed H3K27-altered DMG and 2 patients had a clin-

Table 1
Selected studies reporting on the utility of various PET tracers in the diagnosis or prognostication of pediatric patients with DMG.

Study:	Sample Size:	Main Findings:
^{18}F-FDG: Glucose metabolism		
Zukotynski et al. 2011 [82]	ND: n = 40	• 7/40 with tumor uptake ≥ gray matter. • Patients with uptake in ≥ 50% of the tumor had shorter PFS and OS compared to those with uptake in < 50% of the tumor.
Goda et al. 2013 [83]	n = 11	• No correlation between baseline PET parameters and survival.
Zukotynski et al. 2014 [84]	ND: n = 53 RR: n = 18	• ND DMG: 9/53 with tumor uptake ≥ gray matter. • RR DMG: 1/18 with tumor uptake = gray matter, none with uptake > gray matter. • In ND DMG, correlation of tumor MR CE and ^{18}F-FDG uptake suggested worse OS (P = 0.032), whereas in RR DMG, correlation of MR CE and ^{18}F-FDG uptake suggested more favorable PFS (P = 0.023).
Zukotynski et al. 2017 [85]	n = 33	• Negative correlation between lesional PET and MR ADC pixel values. • A higher negative correlation was associated with a worse PFS.
^{11}C-MET: amino acid uptake		
Rosenfeld et al. 2011 [90]	n = 25 (FDG: n=25; FDG+MET: n=17)	• ^{11}C-MET was marginally more sensitive than ^{18}F-FDG by detecting more lesion sites. • Lack of ^{11}C-MET and ^{18}F-FDG uptake was correlated with an improved survival rate.
Tinkle et al. 2019 [91]	n = 22	• Baseline lesional ^{11}C-MET uptake in 18 /22 patients (82%). • Abnormal ^{11}C-MET uptake extended beyond the conventional MR-defined tumor volume in most patients, but its extent was limited. • Baseline ^{11}C-MET uptake delineates regions at risk for recurrence. • No correlation of PET parameters with survival or treatment outcome.
Pirotte et al. 2007 [86]	n = 14	• Use of PET guidance improved biopsy target selection and provided tumor diagnosis in all trajectories and in all children. • The PET-guided trajectories provided a higher diagnostic yield than those guided by MRI alone.
^{18}F-FET: amino acid uptake		
Marner et al. 2021 [92]	n = 97; H3K27M- mutant DMG n=6	• ^{18}F-FET PET showed significantly higher accuracy for detecting tumor in untreated and treated lesions compared to MRI alone. • The addition of ^{18}F-FET PET to MRI helped discriminate tumor from non-tumor lesions.
^{18}F-DOPA: amino acid uptake		
Piccardo et al. 2019 [93]	n = 22; H3K27M-mutant n = 12; WT n = 10	• Significant differences were noted in MR/MRS parameters (rCBF max, rADC min, Cho/NAA) and PET uptake between H3K27M-mutants and WT (p≤0.02). • T/S ratio on PET can discriminate H3K27M-mutant from WT independently of histology.
Morana et al. 2017 [101]	H3K27M-mutant n=6	• DWI (rADC min), ASL (rCBF max) and PET (T/S, T/N) parameters provide useful complementary information for pediatric diffuse astrocytic tumor grading. • T/S and T/N ratios were independent predictors of PFS.
Morana et al. 2020 [94]	n = 19	• Patients with T/S ratio >1 had an OS ≤12 months and less tumor volume reduction following treatment (p = 0.001). • In all patients, areas of increased PET uptake overlapped with areas of resistance/lack of response to treatment. • T/S ratio was an independent predictor of outcome.
Fiz et al. 2022 [95]	H3K27-altered n = 5; DIPG (clinical or radiologic only) n=2	• All grade 4 gliomas (including DMG) demonstrated a plateau uptake pattern on dynamic PET • TAC shape was an independent predictor of OS, with plateau uptake pattern associated with lower OS compared to accumulation uptake pattern.
^{89}Zr-bevacizumab: VEGF expression		
Jansen et al. 2017 [96]	n = 7	• 5 of 7 primary tumors showed focal uptake. • Considerable intra- and inter-tumoral heterogeneity in delivery. • Positive correlation between MR CE and uptake.
$^{64}CuCl_2$: copper turnover		
Fiz et al. 2022 [100]	n = 8; H3K27-mutant n = 5	• Tracer uptake in tumor areas concordant with MR CE. • 3 out of 5 H3K27-mutant DMGs demonstrated tumor uptake.

Abbreviations: ASL, arterial spin labelling; CE, contrast enhancement; DWI, diffusion-weighted imaging; MR, magnetic resonance; ND, newly diagnosed; OS, overall survival; PET, positron emission tomography; PFS, progression-free survival; rADC, relative apparent diffusion coefficient; rCBF, relative cerebral blood flow; RR, recurrent; TAC, time-activity-curve; T/N, tumor-to-normal tissue; T/S, tumor-to-striatum; WT, wild-type.

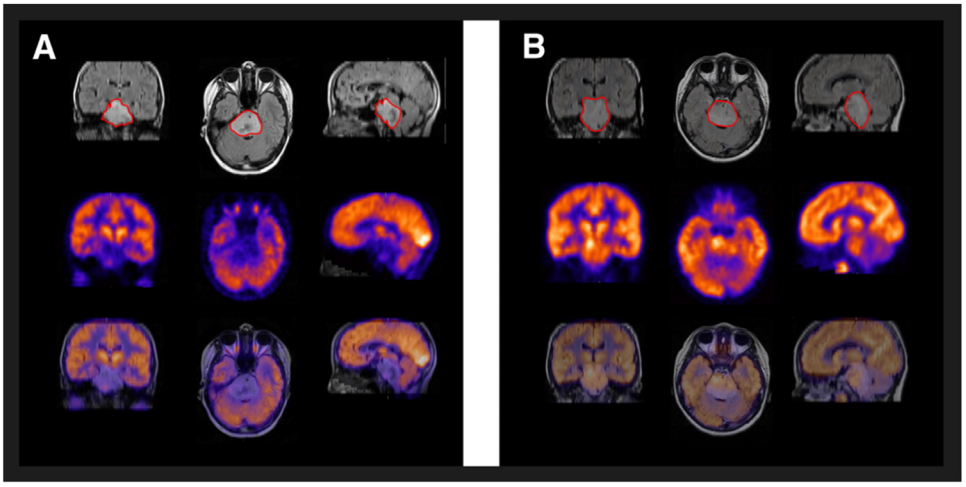

Fig. 2. Illustrative examples of grading scheme for intensity and uniformity of 18F-FDG PET uptake by BSG. (A) 12-y-old girl with intensity of BSG 18F-FDG uptake between normal white and gray matter; percentage of tumor demonstrates 18F-FDG uptake less than 25% (as demonstrated on FLAIR MR image marked with red ROI), PFS of 258 d, and OS of 348 d. (B) 7-y-old boy with intensity of BSG 18F-FDG uptake greater than normal gray matter; percentage of tumor demonstrates 18F-FDG uptake greater than 75% (as demonstrated on FLAIR MR image marked with red ROI), PFS of 169 d, and OS of 196 d. This research was originally published in JNM [82].

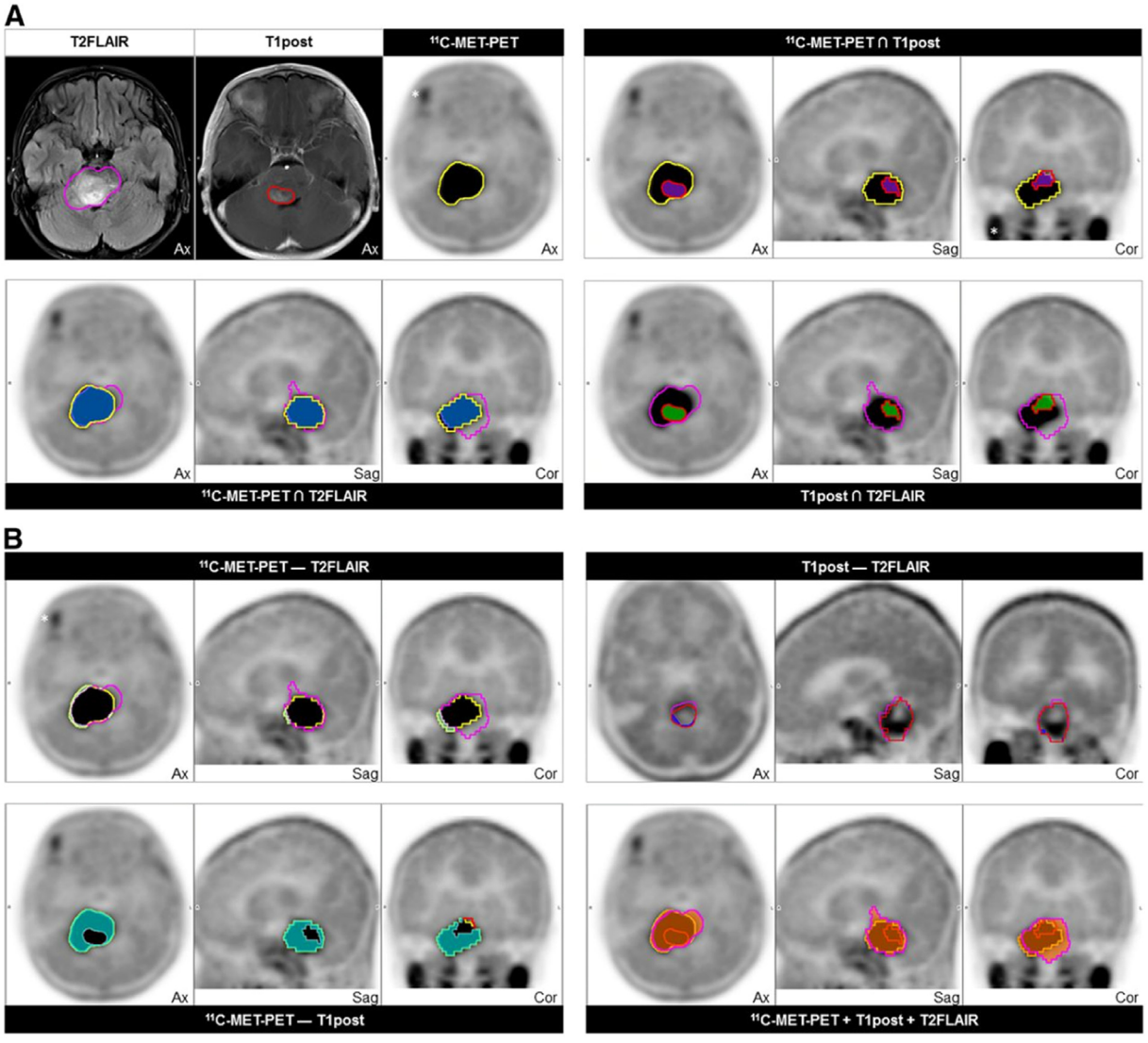

Fig. 3. Example of concordant and discordant segmented tumor volumes based on T2FLAIR (magenta) and T1post (red) abnormalities on MR images and ^{11}C-methionine abnormality (yellow) on ^{11}C-methionine PET. (A) Concordance volumes with coregistered MRI- and ^{11}C-methionine PET–defined tumor (upper left) and indicated concordance volumes (blue = ^{11}C-methionine PET ∩ T2FLAIR; purple = ^{11}C-methionine PET ∩ T1post; green = T1post ∩ T2FLAIR). (B) Indicated discordance volumes (light green = ^{11}C-methionine PET – T2FLAIR; aqua = ^{11}C-methionine PET – T1post; dark blue = T1post – T2FLAIR) and concordant total tumor volume delineated on MRI and ^{11}C-methionine PET (red-orange, bottom right). *Physiologic uptake in exocrine glands. This research was originally published in JNM [91].

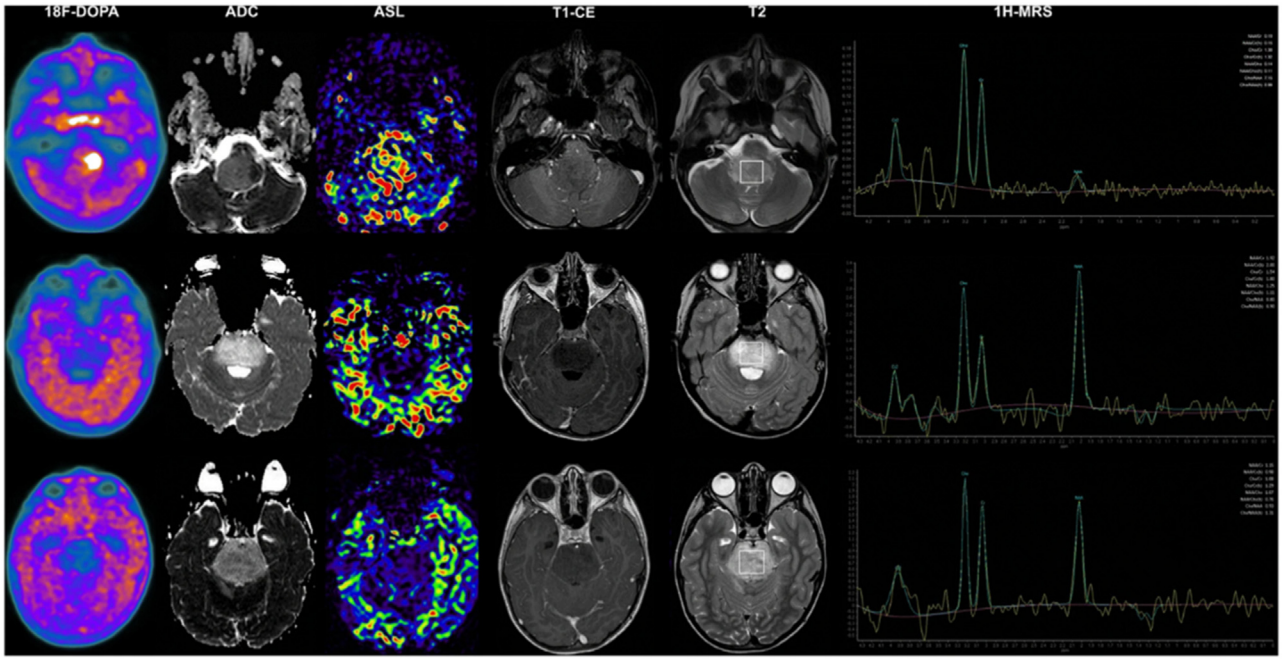

Fig. 4. ^{18}F-DOPA PET and MRI images of H3K27M-mutant and wild-type DMG. Upper row: DMG, H3K27M-m (GB), WHO grade IV (case 4) ^{18}F-DOPA PET shows an area of markedly increased uptake within the lesion (T/N: 2.80; T/S: 1.80). ADC demonstrates a focal area with mildly reduced diffusivity (rADC min: 0.95) on the left side of the lesion corresponding to the ^{18}F-DOPA PET hot spot region. ASL shows increased perfusion (rCBF max: 1.90). Contrast-enhanced (CE) T1-weighted image does not show contrast enhancement. ^{1}H-MRS demonstrates marked increase of Cho/NAA (7.15) and mild increase of Cho/Cr (1.39) ratios. Middle row: Diffuse intrinsic pontine glioma (AA), H3K27M-wt, WHO grade III (case 17) ^{18}F-DOPA PET shows absence of tracer uptake in the lesion (T/N: 1.00; T/S: 0.60). ADC demonstrates increased diffusion (rADC min: 1.42). ASL shows low perfusion (rCBF max: 0.80). CE T1-weighted image does not show contrast enhancement. ^{1}H-MRS demonstrates normal Cho/NAA (0.80) and mild increase of Cho/Cr (1.54) ratios. Of note, this was the only histologically defined high grade glioma which demonstrated lack of increased ^{18}F-DOPA uptake. Lower row: Diffuse intrinsic pontine glioma (DA), H3K27M-wt, WHO grade II (case 21) ^{18}F-DOPA PET shows absence of tracer uptake in the lesion (T/N: 0.95; T/S: 0.45). ADC and ASL images demonstrate increased diffusion (rADC min: 1.26) and low perfusion (rCBF max: 0.78). CE T1-weighted image does not show contrast enhancement. ^{1}H-MRS demonstrates normal Cho/NAA (0.93) and Cho/Cr (1.08) peak area ratios. Note: the box on T2-weighted images indicates the region of interest from which the spectra were acquired. This research was originally published in EJNMMI [93].

ical/radiologic diagnosis of DIPG, analyzed the added value of dynamic ^{18}F-DOPA PET/CT parameters [95]. In this study, the time-activity-curve (TAC) dynamic PET parameter was able to identify patients at higher risk of disease progression and death.

In summary, radiolabeled amino acid-based PET appears to be superior to both ^{18}F-FDG PET and conventional MRI for the detection of DMG, and may delineate more aggressive features as well as provide prognostic information.

Emerging PET tracers

PET imaging with radiolabeled drug derivatives provides an elegant means to quantitatively and noninvasively measure target expression in vivo. This is particularly relevant to DMG, where targeted therapies are being actively investigated, and where the blood-brain-barrier is relatively intact. In this regard, a recent study evaluated ^{89}Zr-labeled bevacizumab in DMG [96]. Bevacizumab is a monoclonal antibody targeting the proangiogenic vascular endothelial growth factor (VEGF), which is frequently overexpressed in DIPG [97]. Five of 7 primary tumors showed focal ^{89}Zr-bevacizumab uptake, with no significant uptake in healthy brain (Figure 5). Inter- and intratumoral heterogeneity of uptake was noted, with ^{89}Zr-bevacizumab uptake present predominantly within MRI contrast-enhanced areas, although uptake in these areas was variable. An autopsy case study confirmed that lesional heterogeneity in ^{89}Zr-bevacizumab uptake on PET correlated with ex vivo measurements [98]. However, PET underestimated the true activity in small lesions due to partial-volume effects.

Copper is a key element in cellular turnover, serves as co-enzyme in various cell functions, including mitochondrial respiration, and plays a key role in cancer metabolism [99]. The cellular uptake of copper is mediated by human copper transporter 1 (CTR1). ^{64}Cu is a "theranostic" radionuclide based on its unique decay scheme, which includes the emission of positrons (suitable for PET imaging) and beta particles and Auger electrons (used in radiotherapy). A recent study in ten pediatric patients with diffuse high-grade gliomas, including 8 DMG, explored the diagnostic utility and dosimetry of ^{64}Cu-chloride ($^{64}CuCl_2$) [100]. In six of the ten patients, tracer uptake in tumor areas correlated with MR contrast enhancement, suggesting that blood–brain barrier damage may be required for its intracranial distribution.

Future directions

Our expanding understanding of metabolic dysregulation in DMG highlights the potential utility of a growing arsenal of metabolic imaging tracers in these tumors. PET tracers targeting metabolic and cell signaling alterations are of interest not only for diagnosis but also to provide a rationale for mechanism-based targeted therapies. There is currently a gap between the metabolic perturbations most prominent in DMG and the metabolic imaging modalities that have been explored clinically in DMG patients. However, several PET tracers relevant to DMG metabolic dysregulation have been investigated in other cancer patients. ^{18}F-PARPi, a tracer that can exploit the metabolic upregulation of PARP enzymes in DMG [31], has shown promise in first-in-human adult brain tumor patients [102], where it may help distinguish between tumor and treatment-related changes. PDGFRA amplifications in DMG may be imaged with a novel radiolabeled small molecule dasatinib derivative being investigated in systemic cancers [103]. ^{18}F-fluoromisonidazole (^{18}F-FMISO) PET, which provides a quantitative non-invasive measure of intratumoral hypoxia levels, has been employed successfully in adult glioma patients [104]. Fi-

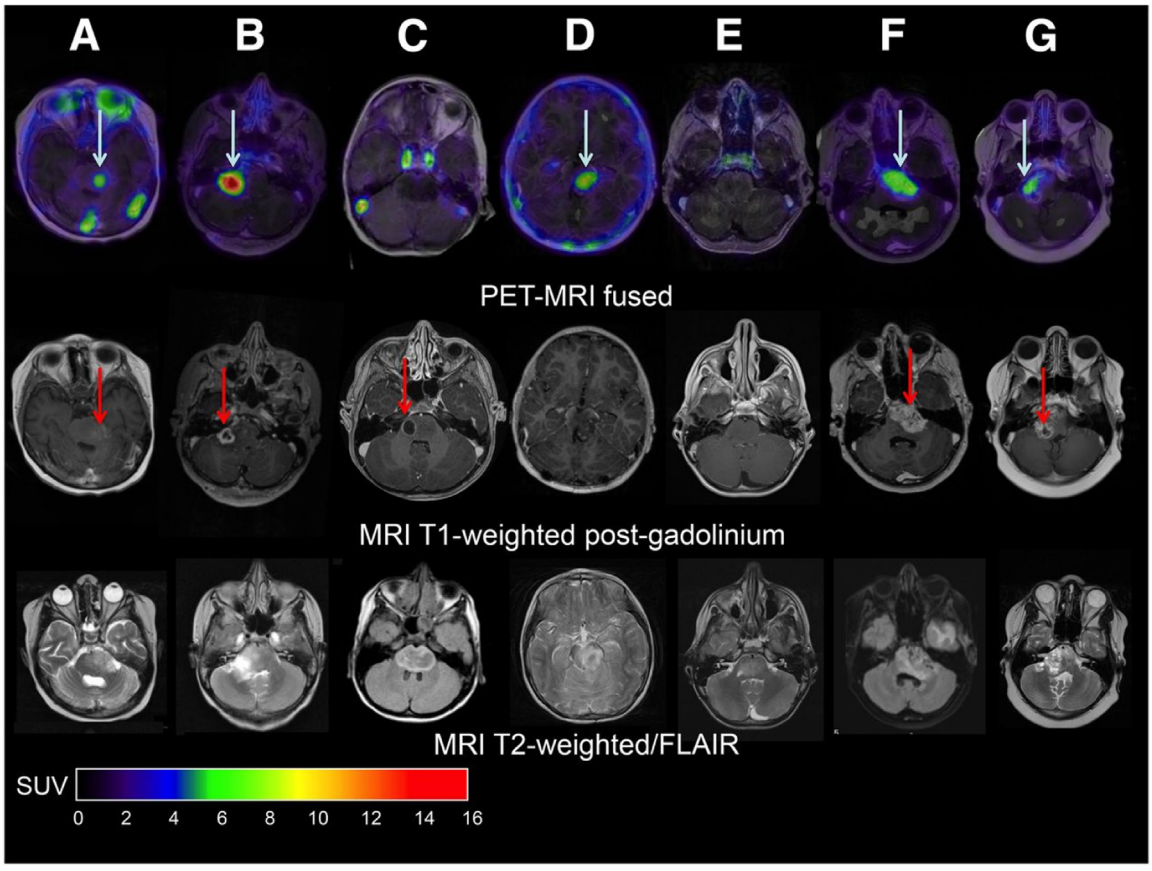

Fig. 5. MR and PET/MR fusion images of patients with DIPG. (Top) ^{89}Zr-bevacizumab PET image (144 h after injection) fused with gadolinium-enhanced T1-weighted MRI image for each patient. (Middle) Gadolinium-enhanced T1-weighted MR images. (Bottom) T2-weighted/fluid-attenuated inversion recovery (FLAIR) MR images. Five tumors showed variable uptake of ^{89}Zr-bevacizumab (blue arrows), with areas within each tumor showing both negative and positive PET results. Two primary tumors (C and E) showed completely negative PET results, whereas T2-weighted images showed tumor infiltration in whole pons of both patients. Red arrows represent areas of contrast enhancement within tumor. In 4 of 5 primary tumors, areas showing positive PET results corresponded to contrast-enhanced areas on MRI (A, B, F, and G). Tumor in C showed MRI contrast-enhanced area but no ^{89}Zr-bevacizumab uptake. Tumor in D showed positive PET results but no gadolinium contrast enhancement on MRI. This research was originally published in JNM [96].

nally, several radiolabeled amino acid tracers have been used to image other brain tumors that may have utility for non-invasively interrogating DMG metabolism. These include ^{18}F-Fluoroglutamine (^{18}F-FGln) [105–107], ^{18}F-Fluorocholine (^{18}F-FCho) [108] and Anti-1-amino-3-[^{18}F]fluorocyclobutane-1- carboxylic acid (^{18}F-fluciclovine, ^{18}F-FACBC) [109]. Glutamine metabolism is an emerging pharmacologic target in gliomas, with several compounds being evaluated in early-stage clinical trials, suggesting a role for glutamine imaging to personalize treatment options [106,107,110]. Using our rapidly expanding knowledge of DMG metabolic vulnerabilities to inform selection of metabolic imaging techniques for clinical investigation may prove beneficial.

Another promising technique for the imaging of DMG metabolism is deuterium metabolic imaging (DMI). This novel, noninvasive approach can generate three-dimensional metabolic maps combining deuterium (^{2}H) MRS with the oral or intravenous administration of nonradioactive ^{2}H-labeled substrates. Furthermore, DMI can trace glucose metabolism beyond its uptake values and provide additional metabolic information through other ^{2}H-labeled substrates [111]. Animal models demonstrated the potential of DMI to provide high-resolution metabolic maps reflecting Warburg effect in gliomas [111]. A recent study showed the capacity of DMI to provide insights on early tumor response to treatment through imaging biomarkers of telomerase reverse transcriptase (TERT) expression [112].

As investigation of these novel metabolic imaging techniques in DMG progresses, it is also important to consider how these techniques might best be integrated into clinical care [113]. Advanced imaging techniques have been explored at many stages in the natural history of DMG, including lesion diagnosis, prognostication and assessment of treatment response. At diagnosis, metabolic imaging may delineate tumor borders to assist radiation planning, define targets for biopsy [114] and even indicate mutational status noninvasively [93]. Imaging parameters may also predict PFS and OS [91,94]. During treatment, serial metabolic imaging may allow more sensitive detection of response to treatment as well as recurrence [115], as metabolic changes may occur in advance of lesion size changes on conventional MRI. It may also be useful in distinguishing true progression from pseudoprogression [116], of particular interest given radiation therapy is the only current standard of care for these tumors and current response assessment guidelines are exclusively based on FLAIR changes [117] which cannot discriminate between these entities. It will be important to develop consensus standardization for how these newer metabolic imaging techniques are performed (as with current guidelines [77]) as well as criteria for interpretation of the results.

The utility of metabolic imaging techniques in DMG may be further enhanced by multimodal combination with other approaches that offer complementary information, such as radiomics and liquid biopsy. Radiomic features extracted from advanced MR sequences, especially MRP, showed good correlation with molecular features in gliomas [48,118]. For instance, radiomic analysis of conventional MR images has been used to investigate K27M mutational status as well as for prognostica-

tion [119]. Radiomic analysis of PET imaging may prove fruitful for DMG in an analogous manner. Liquid biopsy is being increasingly explored in pediatric tumors, including DMG [120], with cell-free DNA (cfDNA) detected in CSF more readily than in plasma. Digital droplet PCR (ddPCR) of CSF cfDNA in DMG has been used for longitudinal assessment of clinical response in clinical trials [121]. Changes in cfDNA preceded radiographic tumor progression by conventional MRI in 50% of DMG patients in the ONC201 trial [122]. Ongoing optimization and standardization of CSF ddPCR in DMG may render it more viable for routine use [123]. Of note, to generate useful combinatorial nomograms requires sufficient patient numbers to generate independent training and validation cohorts. With rare diagnoses such as DMG, collaborative efforts like the CBTN will be critical to amassing these numbers.

Conclusion

Though the mainstay of DMG diagnosis and surveillance, conventional MR imaging is unable to address many relevant clinical questions. Metabolic imaging such as advanced MRI or PET may add valuable information by leveraging our growing understanding of altered metabolism in DMG.

Declaration of Competing Interest

The authors declare that they have no known competing financial interests or personal relationships that could have appeared to influence the work reported in this paper.

CRediT authorship contribution statement

Samantha Lovibond: Conceptualization, Writing – original draft. **Alexandra N. Gewirtz:** Conceptualization, Writing – original draft. **Luca Pasquini:** Writing – original draft. **Simone Krebs:** Conceptualization, Writing – original draft, Writing – review & editing. **Maya S. Graham:** Conceptualization, Writing – original draft, Writing – review & editing.

Funding

S.K. is supported in part by the NIH R37 CA262557, the NIH Lymphoma SPORE Career Enhancement Project Award (P50-CA192937), the MSK Society, the NCATS grant UL1-TR-002384 of the Clinical and Translational Science Center at Weill Cornell Medical College and the TeamConnor Childhood Cancer foundation. M.S.G is supported in part by NIH K08 NS128256, The American Cancer Society CSDG-21-082-01-DMC, The Team Jack Foundation, The Matthew Larson Foundation and the Hyundai Hope on Wheels Foundation. This study was also supported in part by the NIH/NCI Cancer Center Support Grant (P30 CA008748).

References

[1] Q.T. Ostrom, et al., CBTRUS Statistical Report: Primary Brain and Other Central Nervous System Tumors Diagnosed in the United States in 2015-2019, Neuro. Oncol. 24 (Supplement_5) (2022) v1–v95.
[2] D.N. Louis, et al., The 2016 World Health Organization Classification of Tumors of the Central Nervous System: a summary, Acta Neuropathol. 131 (6) (2016) 803–820.
[3] D.N. Louis, et al., The 2021 WHO Classification of Tumors of the Central Nervous System: a summary, Neuro. Oncol. 23 (8) (2021) 1231–1251.
[4] A. Mackay, et al., Molecular, Pathological, Radiological, and Immune Profiling of Non-brainstem Pediatric High-Grade Glioma from the HERBY Phase II Randomized Trial, Cancer Cell 33 (5) (2018) 829–842 e5.
[5] L.M. Hoffman, et al., Clinical, radiologic, pathologic, and molecular characteristics of long-term survivors of diffuse intrinsic pontine glioma (DIPG): a collaborative report from the International and European Society for Pediatric Oncology DIPG Registries, J. Clin. Oncol. 36 (19) (2018) 1963.
[6] L. Zheng, et al., Diffuse Midline Gliomas With Histone H3 K27M Mutation in Adults and Children: A Retrospective Series of 164 Cases, Am. J. Surg. Pathol. 46 (6) (2022) 863.
[7] R. Banan, et al., Diffuse midline gliomas, H3 K27M-mutant are associated with less peritumoral edema and contrast enhancement in comparison to glioblastomas, H3 K27M-wildtype of midline structures, PLoS One 16 (8) (2021) e0249647.
[8] P. Buczkowicz, et al., Histopathological spectrum of paediatric diffuse intrinsic pontine glioma: diagnostic and therapeutic implications, Acta Neuropathol. 128 (4) (2014) 573–581.
[9] D.A. Solomon, et al., Diffuse Midline Gliomas with Histone H3-K27M Mutation: A Series of 47 Cases Assessing the Spectrum of Morphologic Variation and Associated Genetic Alterations, Brain Pathol. 26 (5) (2016) 569–580.
[10] C. Erker, et al., Characteristics of patients >/=10 years of age with diffuse intrinsic pontine glioma: a report from the International DIPG/DMG Registry, Neuro. Oncol. 24 (1) (2022) 141–152.
[11] D. Srikanthan, et al., Diffuse intrinsic pontine glioma: current insights and future directions, Chinese Neurosurgical Journal 7 (1) (2021) 1–11.
[12] T.B. Johung, M. Monje, Diffuse Intrinsic Pontine Glioma: New Pathophysiological Insights and Emerging Therapeutic Targets, Curr. Neuropharmacol. 15 (1) (2017) 88–97.
[13] J.L. Frazier, et al., Treatment of diffuse intrinsic brainstem gliomas: failed approaches and future strategies, J Neurosurg Pediatr 3 (4) (2009) 259–269.
[14] M.S. Graham, I.K. Mellinghoff, Histone-Mutant Glioma: Molecular Mechanisms, Preclinical Models, and Implications for Therapy, Int. J. Mol. Sci. 21 (19) (2020).
[15] A. Mackay, et al., Integrated Molecular Meta-Analysis of 1,000 Pediatric High–Grade and Diffuse Intrinsic Pontine Glioma, Cancer Cell 32 (4) (2017) 520–537 e5.
[16] G. Wu, et al., The genomic landscape of diffuse intrinsic pontine glioma and pediatric non-brainstem high-grade glioma, Nat. Genet. 46 (5) (2014) 444–450.
[17] D. Meyronet, et al., Characteristics of H3 K27M-mutant gliomas in adults, Neuro. Oncol. 19 (8) (2017) 1127–1134.
[18] D.M. Meredith, et al., H3K27-altered diffuse midline gliomas with secondary driver molecular alterations, Cancer Genet. 268 (2022) 33.
[19] R. Banan, et al., Infratentorial IDH-mutant astrocytoma is a distinct subtype, Acta Neuropathol. 140 (4) (2020) 569–581.
[20] L. Zheng, et al., Diffuse Midline Gliomas With Histone H3 K27M Mutation in Adults and Children: A Retrospective Series of 164 Cases, Am. J. Surg. Pathol. 46 (6) (2022) 863–871.
[21] S. Bender, et al., Reduced H3K27me3 and DNA hypomethylation are major drivers of gene expression in K27M mutant pediatric high-grade gliomas, Cancer Cell 24 (5) (2013) 660–672.
[22] B. Krug, et al., Pervasive H3K27 Acetylation Leads to ERV Expression and a Therapeutic Vulnerability in H3K27M Gliomas, Cancer Cell 35 (5) (2019) 782 -+.
[23] S. Nagaraja, et al., Histone Variant and Cell Context Determine H3K27M Reprogramming of the Enhancer Landscape and Oncogenic State, Mol. Cell 76 (6) (2019) 965–980 e12.
[24] S. Venneti, C.B. Thompson, Metabolic Reprogramming in Brain Tumors, Annu Rev Pathol 12 (2017) 515–545.
[25] H. Shen, et al., Targeting reduced mitochondrial DNA quantity as a therapeutic approach in pediatric high-grade gliomas, Neuro. Oncol. 22 (1) (2020) 139–151.
[26] C. Chung, et al., Integrated Metabolic and Epigenomic Reprograming by H3K27M Mutations in Diffuse Intrinsic Pontine Gliomas, Cancer Cell 38 (3) (2020) 334–349 e9.
[27] B.J. Golbourn, et al., Loss of MAT2A compromises methionine metabolism and represents a vulnerability in H3K27M mutant glioma by modulating the epigenome, Nat Cancer 3 (5) (2022) 629–648.
[28] A. Khan, et al., Dual targeting of polyamine synthesis and uptake in diffuse intrinsic pontine gliomas, Nat. Commun. 12 (1) (2021) 971.
[29] S. Pal, et al., A druggable addiction to de novo pyrimidine biosynthesis in diffuse midline glioma, Cancer Cell 40 (9) (2022) 957–972 e10.
[30] N.R. Fons, et al., PPM1D mutations silence NAPRT gene expression and confer NAMPT inhibitor sensitivity in glioma, Nat. Commun. 10 (1) (2019) 3790.
[31] S. Kossatz, et al., Biomarker-Based PET Imaging of Diffuse Intrinsic Pontine Glioma in Mouse Models, Cancer Res. 77 (8) (2017) 2112–2123.
[32] S. Coy, et al., Single cell spatial analysis reveals the topology of immunomodulatory purinergic signaling in glioblastoma, Nat. Commun. 13 (1) (2022) 4814.
[33] J. Tisnado, et al., Conventional and Advanced Imaging of Diffuse Intrinsic Pontine Glioma, J. Child Neurol. 31 (12) (2016) 1386–1393.
[34] J.L. Leach, et al., MR imaging features of diffuse intrinsic pontine glioma and relationship to overall survival: report from the International DIPG Registry, Neuro. Oncol. 22 (11) (2020) 1647–1657.
[35] S. Gururangan, et al., Incidence and patterns of neuraxis metastases in children with diffuse pontine glioma, J. Neurooncol. 77 (2) (2006) 207–212.
[36] D. Rodriguez, et al., MRI and Molecular Characterization of Pediatric High-Grade Midline Thalamic Gliomas: The HERBY Phase II Trial, Radiology 304 (1) (2022) 174–182.
[37] R. Sethi, et al., Prospective neuraxis MRI surveillance reveals a high risk of leptomeningeal dissemination in diffuse intrinsic pontine glioma, J. Neurooncol. 102 (1) (2011) 121–127.
[38] M.S. Aboian, et al., Imaging Characteristics of Pediatric Diffuse Midline Gliomas with Histone H3 K27M Mutation, AJNR Am. J. Neuroradiol. 38 (4) (2017) 795–800.
[39] D. Hargrave, N. Chuang, E. Bouffet, Conventional MRI cannot predict survival in childhood diffuse intrinsic pontine glioma, J. Neurooncol. 86 (3) (2008) 313–319.
[40] S. Thust, et al., Imaging characteristics of H3 K27M histone-mutant diffuse midline glioma in teenagers and adults, Quant Imaging Med Surg 11 (1) (2021) 43–56.
[41] P.K. Lachi, et al., Clinical profile and outcomes in brainstem glioma: An institutional experience, Asian J Neurosurg 10 (4) (2015) 298–302.
[42] D. Gadda, et al., Relationship between Apparent Diffusion Coefficients and MR Spectroscopy Findings in High-Grade Gliomas, J. Neuroimaging 27 (1) (2017) 128–134.

[43] P.S. LaViolette, et al., Precise ex vivo histological validation of heightened cellularity and diffusion-restricted necrosis in regions of dark apparent diffusion coefficient in 7 cases of high-grade glioma, Neuro. Oncol. 16 (12) (2014) 1599–1606.
[44] U. Lobel, et al., Quantitative diffusion-weighted and dynamic susceptibility-weighted contrast-enhanced perfusion MR imaging analysis of T2 hypointense lesion components in pediatric diffuse intrinsic pontine glioma, AJNR Am. J. Neuroradiol. 32 (2) (2011) 315–322.
[45] N. Kathrani, et al., Diffusion and perfusion imaging biomarkers of H3 K27M mutation status in diffuse midline gliomas, Neuroradiology 64 (8) (2022) 1519–1528.
[46] R. Kurokawa, et al., Dynamic susceptibility contrast-MRI parameters, ADC values, and the T2-FLAIR mismatch sign are useful to differentiate between H3-mutant and H3-wild-type high-grade midline glioma, Eur. Radiol. 32 (6) (2022) 3672–3682.
[47] R. Calmon, et al., Radiogenomics of diffuse intrinsic pontine gliomas (DIPGs): correlation of histological and biological characteristics with multimodal MRI features, Eur. Radiol. 31 (12) (2021) 8913–8924.
[48] L. Pasquini, et al., AI and High-Grade Glioma for Diagnosis and Outcome Prediction: Do All Machine Learning Models Perform Equally Well? Front. Oncol. 11 (2021) 601425.
[49] W. Guo, et al., Multiparametric MRI-Based Radiomics Model for Predicting H3 K27M Mutant Status in Diffuse Midline Glioma: A Comparative Study Across Different Sequences and Machine Learning Techniques, Front. Oncol. 12 (2022) 796583.
[50] E. Szychot, et al., Predicting outcome in childhood diffuse midline gliomas using magnetic resonance imaging based texture analysis, J. Neuroradiol. 48 (4) (2021) 243–247.
[51] D. Le Bihan, Theoretical principles of perfusion imaging. Application to magnetic resonance imaging, Invest. Radiol. 27 (1992) S6–11.
[52] G.-H. Jahng, et al., Perfusion magnetic resonance imaging: a comprehensive update on principles and techniques, Korean J. Radiol. 15 (5) (2014) 554–577.
[53] T. Taxt, E. Andersen, R. Jiřík, Single voxel vascular transport functions of arteries, capillaries and veins; and the associated arterial input function in dynamic susceptibility contrast magnetic resonance brain perfusion imaging, Magn. Reson. Imaging 84 (2021) 101–114.
[54] A. Di Costanzo, et al., Spectroscopic, diffusion and perfusion magnetic resonance imaging at 3.0 Tesla in the delineation of glioblastomas: preliminary results, J. Exp. Clin. Cancer Res. 25 (3) (2006) 385.
[55] A. Di Costanzo, et al., Multiparametric 3T MR approach to the assessment of cerebral gliomas: tumor extent and malignancy, Neuroradiology 48 (9) (2006) 622–631.
[56] B.E. McGehee, J.M. Pollock, J.A. Maldjian, Brain perfusion imaging: How does it work and what should I use? J. Magn. Reson. Imaging 36 (6) (2012) 1257–1272.
[57] L. Guo, et al., Diffusion and perfusion weighted magnetic resonance imaging for tumor volume definition in radiotherapy of brain tumors, Radiat. Oncol. 11 (1) (2016) 1–13.
[58] S. Haller, et al., Arterial Spin Labeling Perfusion of the Brain: Emerging Clinical Applications, Radiology 281 (2) (2016) 337–356.
[59] R. Calmon, et al., Cerebral blood flow changes after radiation therapy identifies pseudoprogression in diffuse intrinsic pontine gliomas, Neuro. Oncol. 20 (7) (2018) 994–1002.
[60] A. Romano, et al., Prediction of survival in patients affected by glioblastoma: histogram analysis of perfusion MRI, J. Neurooncol. 139 (2) (2018) 455–460.
[61] J. Juan-Albarracin, et al., Glioblastoma: Vascular Habitats Detected at Preoperative Dynamic Susceptibility-weighted Contrast-enhanced Perfusion MR Imaging Predict Survival, Radiology 287 (3) (2018) 944–954.
[62] M. Bailo, et al., Decoding the Heterogeneity of Malignant Gliomas by PET and MRI for Spatial Habitat Analysis of Hypoxia, Perfusion, and Diffusion Imaging: A Preliminary Study, Front Neurosci 16 (2022) 885291.
[63] H.J. Aronen, et al., High microvascular blood volume is associated with high glucose uptake and tumor angiogenesis in human gliomas, Clin. Cancer Res. 6 (6) (2000) 2189–2200.
[64] N. Sadeghi, et al., Correlation between dynamic susceptibility contrast perfusion MRI and methionine metabolism in brain gliomas: preliminary results, J. Magn. Reson. Imaging 24 (5) (2006) 989–994.
[65] L.W. Kracht, et al., Methyl-[11C]- l-methionine uptake as measured by positron emission tomography correlates to microvessel density in patients with glioma, Eur. J. Nucl. Med. Mol. Imaging 30 (6) (2003) 868–873.
[66] A. Horska, P.B. Barker, Imaging of brain tumors: MR spectroscopy and metabolic imaging, Neuroimaging Clin. N. Am. 20 (3) (2010) 293–310.
[67] D. Bertholdo, A. Watcharakorn, M. Castillo, Brain proton magnetic resonance spectroscopy: introduction and overview, Neuroimaging Clin. N. Am. 23 (3) (2013) 359–380.
[68] S.B. Thakur, et al., Longitudinal MR spectroscopic imaging of pediatric diffuse pontine tumors to assess tumor aggression and progression, AJNR Am. J. Neuroradiol. 27 (4) (2006) 806–809.
[69] E.A. Steffen-Smith, et al., Proton magnetic resonance spectroscopy predicts survival in children with diffuse intrinsic pontine glioma, J. Neurooncol. 105 (2) (2011) 365–373.
[70] K.W. Yeom, et al., Citrate concentrations increase with hypoperfusion in pediatric diffuse intrinsic pontine glioma, J. Neurooncol. 122 (2) (2015) 383–389.
[71] V.Z. Miloushev, K.R. Keshari, A.I. Holodny, Hyperpolarization MRI: preclinical models and potential applications in neuroradiology, Top. Magn. Reson. Imaging. 25 (1) (2016) 31.
[72] L.M. Le Page, et al., Imaging brain metabolism using hyperpolarized 13C magnetic resonance spectroscopy, Trends Neurosci. 43 (5) (2020) 343–354.
[73] I. Park, et al., Development of methods and feasibility of using hyperpolarized carbon-13 imaging data for evaluating brain metabolism in patient studies, Magn. Reson. Med. 80 (3) (2018) 864–873.
[74] V.Z. Miloushev, et al., Metabolic Imaging of the Human Brain with Hyperpolarized (13)C Pyruvate Demonstrates (13)C Lactate Production in Brain Tumor Patients, Cancer Res. 78 (14) (2018) 3755–3760.
[75] A.W. Autry, et al., Pilot Study of Hyperpolarized (13)C Metabolic Imaging in Pediatric Patients with Diffuse Intrinsic Pontine Glioma and Other CNS Cancers, AJNR Am. J. Neuroradiol. 42 (1) (2021) 178–184.
[76] S. Krebs, et al., Positron emission tomography and magnetic resonance imaging in primary central nervous system lymphoma-a narrative review, Ann Lymphoma 5 (2021).
[77] A. Piccardo, et al., Joint EANM/SIOPE/RAPNO practice guidelines/SNMMI procedure standards for imaging of paediatric gliomas using PET with radiolabelled amino acids and [(18)F]FDG: version 1.0, Eur. J. Nucl. Med. Mol. Imaging 49 (11) (2022) 3852–3869.
[78] R. Boellaard, et al., FDG PET and PET/CT: EANM procedure guidelines for tumour PET imaging: version 1.0, Eur. J. Nucl. Med. Mol. Imaging 37 (1) (2010) 181–200.
[79] S.T. Treves, et al., 2016 update of the North American consensus guidelines for pediatric administered radiopharmaceutical activities, Soc Nuclear Med (2016).
[80] EANM Dosage Card (Version 5.7.2016). 2016; Available from: https://www.eanm.org/docs/EANM_Dosage_Card_040214.pdf.
[81] M. Ollivier, et al., P2X-GCaMPs as Versatile Tools for Imaging Extracellular ATP Signaling, eNeuro 8 (1) (2021) p. ENEURO.0185-20.2020.
[82] K.A. Zukotynski, et al., Evaluation of 18F-FDG PET and MRI associations in pediatric diffuse intrinsic brain stem glioma: a report from the Pediatric Brain Tumor Consortium, J. Nucl. Med. 52 (2) (2011) 188–195.
[83] J.S. Goda, et al., Can multiparametric MRI and FDG-PET predict outcome in diffuse brainstem glioma? A report from a prospective phase-II study, Pediatr. Neurosurg. 49 (5) (2013) 274–281.
[84] K. Zukotynski, et al., 18F-FDG PET and MR imaging associations across a spectrum of pediatric brain tumors: a report from the pediatric brain tumor consortium, J. Nucl. Med. 55 (9) (2014) 1473–1480.
[85] K.A. Zukotynski, et al., Correlation of (18)F-FDG PET and MRI Apparent Diffusion Coefficient Histogram Metrics with Survival in Diffuse Intrinsic Pontine Glioma: A Report from the Pediatric Brain Tumor Consortium, J. Nucl. Med. 58 (8) (2017) 1264–1269.
[86] B.J. Pirotte, et al., Results of positron emission tomography guidance and reassessment of the utility of and indications for stereotactic biopsy in children with infiltrative brainstem tumors, J. Neurosurg. 107 (5 Suppl) (2007) 392–399.
[87] S. Goldman, et al., Regional glucose metabolism and histopathology of gliomas. A study based on positron emission tomography-guided stereotactic biopsy, Cancer 78 (5) (1996) 1098–1106.
[88] O. Yanagida, et al., Human L-type amino acid transporter 1 (LAT1): characterization of function and expression in tumor cell lines, Biochim. Biophys. Acta 1514 (2) (2001) 291–302.
[89] T. Lahoutte, et al., SPECT and PET amino acid tracer influx via system L (h4F2hc-hLAT1) and its transstimulation, J. Nucl. Med. 45 (9) (2004) 1591–1596.
[90] A. Rosenfeld, et al., Use of positron emission tomography in the evaluation of diffuse intrinsic brainstem gliomas in children, J. Pediatr. Hematol. Oncol. 33 (5) (2011) 369–373.
[91] C.L. Tinkle, et al., Evaluation of (11)C-Methionine PET and Anatomic MRI Associations in Diffuse Intrinsic Pontine Glioma, J. Nucl. Med. 60 (3) (2019) 312–319.
[92] L. Marner, et al., Diagnostic accuracy and clinical impact of [18F]FET PET in childhood CNS tumors, Neuro. Oncol. 23 (12) (2021) 2107–2116.
[93] A. Piccardo, et al., Advanced MR imaging and (18)F-DOPA PET characteristics of H3K27M-mutant and wild-type pediatric diffuse midline gliomas, Eur. J. Nucl. Med. Mol. Imaging 46 (8) (2019) 1685–1694.
[94] G. Morana, et al., Correlation of multimodal (18)F-DOPA PET and conventional MRI with treatment response and survival in children with diffuse intrinsic pontine gliomas, Theranostics 10 (26) (2020) 11881–11891.
[95] F. Fiz, et al., Role of Dynamic Parameters of 18F-DOPA PET/CT in Pediatric Gliomas, Clin. Nucl. Med. 47 (6) (2022) 517–524.
[96] M.H. Jansen, et al., Molecular Drug Imaging: (89)Zr-Bevacizumab PET in Children with Diffuse Intrinsic Pontine Glioma, J. Nucl. Med. 58 (5) (2017) 711–716.
[97] S. Puget, et al., Mesenchymal transition and PDGFRA amplification/mutation are key distinct oncogenic events in pediatric diffuse intrinsic pontine gliomas, PLoS One 7 (2) (2012) e30313.
[98] S.E.M. Veldhuijzen van Zanten, et al., Multiregional Tumor Drug-Uptake Imaging by PET and Microvascular Morphology in End-Stage Diffuse Intrinsic Pontine Glioma, J. Nucl. Med. 59 (4) (2018) 612–615.
[99] D.C. Brady, et al., Copper is required for oncogenic BRAF signalling and tumorigenesis, Nature 509 (7501) (2014) 492–496.
[100] F. Fiz, et al., Diagnostic and Dosimetry Features of [(64)Cu]CuCl2 in High-Grade Paediatric Infiltrative Gliomas, Mol. Imaging Biol. (2022).
[101] G. Morana, et al., Grading and outcome prediction of pediatric diffuse astrocytic tumors with diffusion and arterial spin labeling perfusion MRI in comparison with 18F-DOPA PET, Eur. J. Nucl. Med. Mol. Imaging 44 (12) (2017) 2084–2093.
[102] R.J. Young, et al., Preclinical and first-in-human-brain-cancer applications of [(18)F]poly (ADP-ribose) polymerase inhibitor PET/MR, Neurooncol Adv 2 (1) (2020) vdaa119.
[103] S. Krebs, et al., First-in-Humans Trial of Dasatinib-Derivative Tracer for Tumor Kinase-Targeted PET, J. Nucl. Med. 61 (11) (2020) 1580–1587.
[104] S. Collet, et al., Simultaneous Mapping of Vasculature, Hypoxia, and Proliferation Using Dynamic Susceptibility Contrast MRI, (18)F-FMISO PET, and (18)F-FLT PET

in Relation to Contrast Enhancement in Newly Diagnosed Glioblastoma, J. Nucl. Med. 62 (10) (2021) 1349–1356.
[105] S. Venneti, et al., Glutamine-based PET imaging facilitates enhanced metabolic evaluation of gliomas in vivo, Sci. Transl. Med. 7 (274) (2015) p. 274ra17-274ra17.
[106] M. Grkovski, et al., Pharmacokinetic Assessment of (18)F-(2S,4R)-4-Fluoroglutamine in Patients with Cancer, J. Nucl. Med. 61 (3) (2020) 357–366.
[107] J. Sponagel, et al., Sex differences in brain tumor glutamine metabolism reveal sex-specific vulnerabilities to treatment, Med (N Y) (2022).
[108] A.M. García Vicente, et al., 18F-Fluorocholine PET/CT in the Prediction of Molecular Subtypes and Prognosis for Gliomas, Clin. Nucl. Med. 44 (10) (2019) e548–e558.
[109] L. Michaud, et al., (18)F-Fluciclovine ((18)F-FACBC) PET imaging of recurrent brain tumors, Eur. J. Nucl. Med. Mol. Imaging 47 (6) (2020) 1353–1367.
[110] M.G. Vander Heiden, Targeting cancer metabolism: a therapeutic window opens, Nat Rev Drug Discov 10 (9) (2011) 671–684.
[111] H.M. De Feyter, et al., Deuterium metabolic imaging (DMI) for MRI-based 3D mapping of metabolism in vivo, Sci. Adv. 4 (8) (2018) eaat7314.
[112] G. Batsios, et al., Deuterium Metabolic Imaging Reports on TERT Expression and Early Response to Therapy in Cancer, Clin. Cancer Res. 28 (16) (2022) 3526–3536.
[113] M.M. Kim, et al., Non-invasive metabolic imaging of brain tumours in the era of precision medicine, Nat. Rev. Clin. Oncol. 13 (12) (2016) 725–739.
[114] M. Preuss, et al., Integrated PET/MRI for planning navigated biopsies in pediatric brain tumors, Childs Nerv. Syst. 30 (8) (2014) 1399–1403.
[115] A.K. Bag, et al., (11)C-Methionine PET for Identification of Pediatric High-Grade Glioma Recurrence, J. Nucl. Med. 63 (5) (2022) 664–671.
[116] L. Marner, et al., Early Postoperative (18)F-FET PET/MRI for Pediatric Brain and Spinal Cord Tumors, J. Nucl. Med. 60 (8) (2019) 1053–1058.
[117] T.M. Cooney, et al., Response assessment in diffuse intrinsic pontine glioma: recommendations from the Response Assessment in Pediatric Neuro-Oncology (RAPNO) working group, Lancet Oncol. 21 (6) (2020) e330–e336.
[118] L. Pasquini, et al., Deep Learning Can Differentiate IDH-Mutant from IDH-Wild GBM, J Pers Med 11 (4) (2021).
[119] L.T. Tam, et al., MRI-based radiomics for prognosis of pediatric diffuse intrinsic pontine glioma: an international study, Neurooncol Adv 3 (1) (2021) vdab042.
[120] A.M. Miller, et al., Next-generation Sequencing of Cerebrospinal Fluid for Clinical Molecular Diagnostics in Pediatric, Adolescent and Young Adult (AYA) Brain Tumor Patients, Neuro. Oncol. (2022).
[121] E. Panditharatna, et al., Clinically Relevant and Minimally Invasive Tumor Surveillance of Pediatric Diffuse Midline Gliomas Using Patient-Derived Liquid Biopsy, Clin. Cancer Res. 24 (23) (2018) 5850–5859.
[122] E. Cantor, et al., Serial H3K27M cell-free tumor DNA (cf-tDNA) tracking predicts ONC201 treatment response and progression in diffuse midline glioma, Neuro. Oncol. 24 (8) (2022) 1366–1374.
[123] D. Li, et al., Standardization of the liquid biopsy for pediatric diffuse midline glioma using ddPCR, Sci. Rep. 11 (1) (2021) 5098.